

# RiboFlow: Conditional *De Novo* RNA Sequence-Structure Co-Design via Synergistic Flow Matching

Runze Ma<sup>\*1</sup> Zhongyue Zhang<sup>\*1</sup> Zichen Wang<sup>1</sup> Chenqing Hua<sup>2</sup> Zhuomin Zhou<sup>1</sup>  
Fenglei Cao<sup>3</sup> Jiahua Rao<sup>4</sup> Shuangjia Zheng<sup>1</sup>

## Abstract

Ribonucleic acid (RNA) binds to molecules to achieve specific biological functions. While generative models are advancing biomolecule design, existing methods for designing RNA that target specific ligands face limitations in capturing RNA's conformational flexibility, ensuring structural validity, and overcoming data scarcity. To address these challenges, we introduce RiboFlow, a synergistic flow matching model to co-design RNA structures and sequences based on target molecules. By integrating RNA backbone frames, torsion angles, and sequence features in an unified architecture, RiboFlow explicitly models RNA's dynamic conformations while enforcing sequence-structure consistency to improve validity. Additionally, we curate RiboBind, a large-scale dataset of RNA-molecule interactions, to resolve the scarcity of high-quality structural data. Extensive experiments reveal that RiboFlow not only outperforms state-of-the-art RNA design methods by a large margin but also showcases controllable capabilities for achieving high binding affinity to target ligands. Our work bridges critical gaps in controllable RNA design, offering a framework for structure-aware, data-efficient generation.

## 1. Introduction

Ribonucleic acid (RNA) is a programmable biomolecule that achieves precise molecular recognition through its dynamic three-dimensional structure (Wong et al., 2024),

<sup>\*</sup>Equal contribution <sup>1</sup>Global Institute of Future Technology, Shanghai Jiao Tong University, Shanghai, China <sup>2</sup>School of Computer Science, McGill University, Montreal, Canada <sup>3</sup>Shanghai Academy of AI for Science, Shanghai, China <sup>4</sup>School of Computer Science and Engineering, Sun Yat-sen University, Guangzhou, China. Correspondence to: Shuangjia Zheng <shuangjia.zheng@sjtu.edu.cn>.

enabling applications in catalysis, biosensing, and therapeutic targeting (Wilson & Lilley, 2021; Cao et al., 2024). Advances in computational tools, exemplified by AlphaFold3 (Abramson et al., 2024), have revolutionized biomolecular structure prediction, while generative models (Lin et al., 2024; Zambaldi et al., 2024; Hua et al., 2024; Wang et al., 2024) now pioneer the design of *de novo* biomolecules with specific binding properties. RNA, with its structural flexibility at the tertiary level, ease of chemical synthesis in laboratory settings, and low immunogenicity in biological systems, stands out as a promising candidate for therapeutic drugs and biochemical reagents (Sun et al., 2020; Disney et al., 2022). However, existing methods for designing RNAs that bind specific small molecules—critical for therapeutic and diagnostic applications—face unresolved challenges at the intersection of data availability, interaction modeling, and structural validity.

Recent work has laid foundations for RNA design. Tools like RNAiFold (Dotu et al., 2014) and gRNAde (Joshi et al., 2024) generate sequences matching predefined secondary or tertiary structures, while RNA-FrameFlow (Anand et al., 2024), MMDiff (Morehead et al., 2023), and RNAFlow (Nori & Jin, 2024) focus on backbone generation. Yet, designing RNA for small-molecule targeting remains an open problem due to three gaps: (1) the inherent conformational flexibility of RNA requires the simultaneous and consistent consideration of both its structure and sequence (Falese et al., 2021); (2) existing models lack explicit conditioning on ligand geometry, limiting their ability to capture RNA-ligand binding dynamics; and (3) the scarcity of RNA-ligand structural data restricts the scalability and generalizability of data-driven approaches.

To bridge these gaps, we identify three key challenges. First, ensuring generated RNAs satisfy both binding specificity and biophysical validity requires co-designing sequence and structure in a synergistic framework. Second, modeling RNA's structural flexibility—particularly its torsion angles and backbone dynamics—while preserving sequence-structure compatibility remains a complex geometric and thermodynamic problem. Third, the absence of large-scale, standardized RNA-ligand interaction datasets hinders train-

ing robust generative models.

We try to address these challenges. For model design, we introduce **RiboFlow**, a synergistic flow matching model for *de novo* RNA discrete sequence and continuous structure co-design. By conditioning on ligand geometry and leveraging RNA backbone frames, torsion angles, and sequence features, RiboFlow models conformational flexibility while enforcing sequence-structure consistency. A novel co-design pre-training strategy is proposed to further enhance geometric awareness by distilling structural priors from RNA crystal structures. To overcome data scarcity, we introduce **RiboBind**, a comprehensive dataset of RNA-ligand complexes systematically curated from the PDB database, comprising 1,591 RNA-ligand complexes and 3,012 RNA-ligand pairs.

Our contributions are: (i) **Task Formulation**: We propose a first-of-its-kind synergistic flow-matching framework for ligand-conditioned *de novo* RNA design. The model incorporates torsion angle and backbone frame modeling, enabling sequence-structure co-design for specified ligands while offering controllable ligand-binding specificity. (ii) **Dataset**: We present RiboBind, the largest standardized RNA-ligand interaction benchmark, enabling data-driven RNA discovery. (iii) **Evaluation**: We develop a multi-faceted pipeline assessing structural validity and binding affinity (via docking and scoring). Experimental results demonstrate that RiboFlow outperforms state-of-the-art RNA design methods by a large margin (e.g., achieving a 2.2-fold improvement in the AF3 binding metric and a 50% increase in validity), but also showcases controllable capabilities for achieving high binding affinity to target ligands. We anticipate this work advancing RNA design toward structure-aware, ligand-conditioned design, with promising applications in therapeutics and synthetic biology.

## 2. Related Work

### 2.1. RNA Design

Recently, the rise of deep learning has greatly advanced biomolecular design, leading to extensive attention in RNA design. Currently, RNA design can be broadly categorized into two main approaches: sequence-based and structure-based methods. *Sequence-based design* primarily aims to address the RNA inverse folding problem, which involves designing an RNA sequence that folds into a desired RNA structure. While early efforts (Dotu et al., 2014; Yang et al., 2017; Churkin et al., 2018; Runge et al., 2019) largely focus on RNA secondary structure information, recent studies (Tan et al., 2024; Joshi et al., 2024; Huang et al., 2024; Wong et al., 2024) begin to explore the use of RNA 3D structural information to guide sequence design. On the other hand, *structure-based design*, still in its early

stages, encompasses approaches such as RNA backbone design (Anand et al., 2024), which enables the creation of RNA with specific structures. Another approach is RNA-protein co-design (Morehead et al., 2023; Nori & Jin, 2024), which focuses on designing RNA and protein components by accounting for their interactions. However, these methods are not capable of designing ligand-targeting RNAs, limiting their applications in broader diagnostic and synthetic biology scenarios.

### 2.2. Flow Matching

Flow matching (Lipman et al., 2023; Liu et al., 2023), an emerging generative modeling approach, is increasingly recognized as a compelling alternative to traditional generative models (Kingma, 2014; Goodfellow et al., 2014; Ho et al., 2020). It has extensive applications in both the computer vision and natural language processing fields (Dao et al., 2023; Gat et al., 2024; Esser et al., 2024). Within the realm of biomolecular design, the focus of this paper, researchers are actively exploring the application of flow matching for diverse molecular design tasks. For example, several studies (Zhang et al., 2024; Yim et al., 2023; Bose et al., 2024) utilize SE(3)-equivariant flow models to design small molecules and proteins, while others (Huguet et al., 2024; Campbell et al., 2024) integrate protein sequence for protein design, or leverage multiple sequence alignment (MSA) coevolutionary information (Hua et al., 2024; Wang et al., 2024) to design enzymes and antibodies. In contrast to these methods, RiboFlow integrates RNA-specific structural priors with sequence-structure consistency through synergistic flow matching, thereby deriving the benefits of both data-efficient representations for RNA inputs.

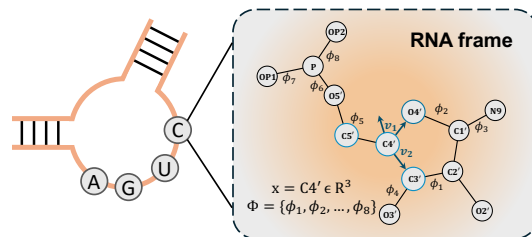


Figure 1: RNA backbone parameterization. Using the  $C4'$  atom as the origin, a local coordinate system is established using  $v_1$  and  $v_2$  defined by vectors along the  $C4'-O4'$  and  $C4'-C3'$  bonds via the Gram-Schmidt process. The remaining atoms are then parameterized by 8 torsion angles  $\Phi$ .

## 3. Preliminary

**RNA Backbone Parameterization.** As illustrated in Figure 1, an RNA has a backbone made of alternating phosphate groups ( $P$ ,  $OP1$ ,  $OP2$ ,  $O5'$ ) and the sugar ribose ( $C1'$  -  $C5'$ ,  $O2'$ ,  $O3'$ ,  $O4'$ ). A nitrogen atom, located at the base

attachment site ( $N9$  of purines or  $N1$  of pyrimidines), is often included in modeling. Utilizing recent RNA parameterization methods (Morehead et al., 2023; Anand et al., 2024), we construct a local coordinate system for each nucleotide based on the  $C4'$ ,  $C3'$ , and  $O4'$  atoms of the ribose. The positions of the remaining atoms are then determined by a set of eight torsion angles,  $\Phi = \{\phi_i\}_{i=1}^8$ , where  $\phi_i \in \mathbb{R}^2$ , along with bond lengths and bond angles (Gelbin et al., 1996). This parameterized approach can effectively captures the conformational flexibility of RNA.

**Notations and Problem Formulation.** We consider a binding system comprising an RNA-ligand pair  $\mathcal{C} = \{\mathcal{T}, \mathcal{M}\}$ , where the RNA, denoted by  $\mathcal{T}$ , consists of  $N_t$  nucleotides, and the ligand, denoted by  $\mathcal{M}$ , consists of  $N_m$  atoms. The 3D geometry of the ligand is represented as  $\mathcal{M} = \{(a^{(i)}, b^{(i)})\}_{i=1}^{N_m}$ , where  $a^{(i)} \in \mathbb{R}^{n_m}$  indicate the atom type ( $n_m$  is the total number of possible atom types), and  $b^{(i)} \in \mathbb{R}^3$  denotes its 3D Cartesian coordinates. The RNA is represented by the backbone atoms of each nucleotide, and is parameterized as a set of nucleotide blocks  $T^{(i)} = \{x^{(i)}, r^{(i)}, c^{(i)}\}$ . Here,  $x^{(i)} \in \mathbb{R}^3$  is the position of the  $C4'$  atom of the  $i$ -th nucleotide,  $r^{(i)} \in \text{SO}(3)$  is a rotation matrix defining the orientation of the local frame formed by  $C3' - C4' - O4'$  relative to a global reference frame, and  $c^{(i)} \in \{A, C, G, U\}$  represents the nucleotide type. The complete RNA structure is represented by  $\mathcal{T} = \{T^{(i)}\}_{i=1}^{N_t}$ . Our goal is to develop a probabilistic model that learns the conditional distribution  $p(\mathcal{T}|\mathcal{M})$ , i.e., generating an RNA  $\mathcal{T}$  conditioned on a target ligand structure  $\mathcal{M}$ .

## 4. Methods

In this section, we present RiboFlow, a flow matching framework for *de novo* RNA design conditioned on target small molecules. RiboFlow operates in two key stages: *initially*, it learns a distribution of structurally plausible RNAs during a synergistic co-design pre-training stage, establishing priors for molecule-conditioned generation. *Subsequently*, it is trained to generate high-affinity RNAs given a specific target molecule. For clarity, a comprehensive overview of the flow matching is discussed in the Appendix C, with mathematical tools and proofs used in our methodology. The architecture of RiboFlow is illustrated in Figure 2.

### 4.1. Overview

As mentioned in the preliminaries, the  $i$ -th nucleotide in an RNA can be parameterized as  $T^{(i)} = \{x^{(i)}, r^{(i)}, c^{(i)}\}$ . We use time  $t = 1$  to represent the target data (i.e., the real RNA data  $\mathcal{T}_1$ ), and  $t = 0$  to represent noise data (i.e.,  $\mathcal{T}_0$ ). Inspired by recent work of (Yim et al., 2023; Campbell et al., 2024), the conditional flow  $p_t(\mathcal{T}|\mathcal{T}_1)$  in the RNA generation

process for a time step  $t \in [0, 1]$  can be expressed as:

$$p_t(\mathcal{T}|\mathcal{T}_1) = \prod_{i=1}^{N_t} p_t(x_t^{(i)}|x_1^{(i)}) p_t(r_t^{(i)}|r_1^{(i)}) p_t(c_t^{(i)}|c_1^{(i)}), \quad (1)$$

where  $N_t$  denotes the length of the RNA sequence. The above formula allows us to synergistically consider the probability distributions of the three parts (translation, rotation, and nucleotide type) during training and sampling, thereby modeling the RNA generation process into the SE(3) space and the nucleotide type space, respectively.

### 4.2. RiboFlow on SE(3)

We model RNA structure in SE(3) space using a set of structure frames, denoted as  $\mathbf{F} = \{(x^{(i)}, r^{(i)})\}_{i=1}^{N_t}$ , where  $x^{(i)} \in \mathbb{R}^3$  represents the translation and  $r^{(i)} \in \text{SO}(3)$  represents the rotation of the  $i$ -th nucleotide. We define a forward process that transforms an initial noisy frame set  $F_0 \sim p_0(F_0)$  to a target structure frame set  $F_1 \sim p_1(F_1)$ . A continuous flow  $F_t$  between  $F_0$  and  $F_1$  is constructed by interpolating on the SE(3) manifold:

$$F_t = \exp_{F_0}(t \cdot \log_{F_0}(F_1)). \quad (2)$$

Here,  $\exp(\cdot)$  and  $\log(\cdot)$  are the exponential and logarithmic maps respectively, enabling movement along the curved SE(3) manifold. Since the SE(3) can be decomposed into independent translations and rotations, we can also obtain the closed-form interpolations (Yim et al., 2023) for  $\mathbb{R}^3$  and SO(3) separately:

$$x_t = (1 - t)x_0 + tx_1; \quad (3)$$

$$r_t = \exp_{r_0}(t \cdot \log_{r_0}(r_1)), \quad (4)$$

where  $x_0$  sampled from  $\mathcal{N}(0, \mathbf{I})$ , and  $r_0$  sampled uniformly from the rotation group SO(3), denoted as  $\mathcal{U}(\text{SO}(3))$ . Based on these interpolations, we can derive the conditional vector fields  $u_t$  for the translation and rotation components respectively (Tong et al., 2024) due to their simple nature:

$$u_t(x_t^{(i)}|x_1^{(i)}, x_0^{(i)}) = x_1^{(i)} - x_0^{(i)}; \quad (5)$$

$$u_t(r_t^{(i)}|r_1^{(i)}, r_0^{(i)}) = \log_{r_t^{(i)}}(r_1^{(i)}). \quad (6)$$

Hence, we leverage an SE(3)-equivariant neural network  $v_\theta(\cdot)$  to regress the conditional vector fields at time  $t$ . For  $N_t$  structure frames, the loss to train the conditional flow matching for translation can be written as follows:

$$\mathcal{L}_{\text{trans}} = \mathbb{E}_{t \sim \mathcal{U}(0,1), p_1(x_1), p_0(x_0), p_t(x_t|x_0, x_1)} \sum_{i=1}^{N_t} \left\| v_\theta^{(i)}(x_t, t) - x_1^{(i)} + x_0^{(i)} \right\|_{\mathbb{R}^3}^2, \quad (7)$$

and the loss to train rotation conditional flow matching is:

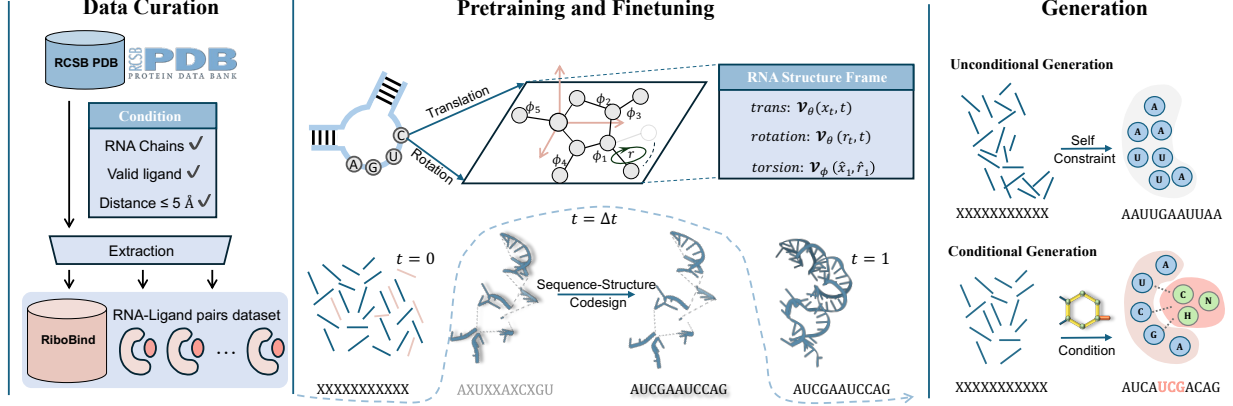


Figure 2: Framework of RiboFlow. We start by collecting and constructing RiboBind, a large-scale RNA-ligand interaction dataset, from the RCSB PDB database. RiboFlow is then pretrained on RNAsolo using a sequence-structure synergistic co-design strategy to enhance its geometric awareness. Next, the model is fine-tuned with RiboBind, enabling it to design RNAs with high affinity under ligand constraints. During inference, RiboFlow generates structurally valid and high-affinity RNAs tailored to different ligands. In the figure, “X” represents uncertain nucleotides.

$$\mathcal{L}_{\text{rot}} = \mathbb{E}_{t \sim \mathcal{U}(0,1), p_1(r_1), p_0(r_0), p_t(r_t|r_0, r_1)} \sum_{i=1}^{N_t} \left\| \mathbf{v}_{\theta}^{(i)}(r_t, t) - \frac{\log_{r_t^{(i)}}(r_1^{(i)})}{1-t} \right\|_{\text{SO}(3)}^2. \quad (8)$$

At the same time, according to Equations 5 and 6, we can obtain the predicted structure frame  $\hat{F}_1 = \{(\hat{x}_1^{(i)}, \hat{r}_1^{(i)})\}_{i=1}^{N_t}$  given the corrupted structure frame  $F_t$ .

### 4.3. RiboFlow on Torsion Angles

The conformational flexibility of the RNA backbone is largely determined by its 8 torsion angles. These angles,  $\phi \in \Phi$ , which are elements of  $\mathbb{R}^2$ , require appropriate constraints to generate physically plausible RNA structures.

Existing studies have explored modeling torsion angles on the torus (Lin et al., 2024) and demonstrated promising experimental results. However, such an approach may increase computational complexity when regressing conditional vector fields of torsion angles. Hence, we introduce a torsion angle prediction module, denoted as  $\mathbf{v}_{\phi}(\cdot)$ . This module employs a shallow ResNet architecture (He et al., 2016), which is first implemented in the structure prediction module of AlphaFold2 (Jumper et al., 2021) and has been widely adopted in recent works. By utilizing the predicted structural frames  $\hat{F}_1 = \{(\hat{x}_1^{(i)}, \hat{r}_1^{(i)})\}_{i=1}^{N_t}$ , the module can predict the ground-truth torsion angles  $\Phi_1$  directly. The process can be formulated as follows:

$$\hat{\Phi}_1^{(i)} = \mathbf{v}_{\phi}(\hat{x}_1^{(i)}, \hat{r}_1^{(i)}). \quad (9)$$

Here,  $\hat{\Phi}_1^{(i)}$  represents the predicted set of 8 torsion angles for the  $i$ -th nucleotide. The loss between the predicted and

true torsion angles can be formulated as:

$$\mathcal{L}_{\text{tors}} = \frac{1}{8N_t} \sum_{i=1}^{N_t} \sum_{\phi \in \Phi_1^{(i)}, \hat{\phi} \in \hat{\Phi}_1^{(i)}} \left\| \hat{\phi} - \phi \right\|_{\mathbb{R}^2}^2. \quad (10)$$

### 4.4. RiboFlow on Nucleotide Type

The intricate interplay between sequence and structure in RNA molecules necessitates a generation process that can effectively capture and leverage their mutual constraints. To address this, we introduce a synergistic flow matching approach that integrates the semantic information of the sequence with the structural flexibility inherent to RNA. This method not only constrains the generation process but also ensures that the generated sequences are biologically plausible and functionally relevant. For an RNA sequence  $c = \{c^{(i)}\}_{i=1}^{N_t}$ , we define  $c_t^{(i)} \sim p(s_t^{(i)})$ , where  $s_t^{(i)}$  is a probability vector representing the distribution over nucleotide types, following a multinomial distribution.

Following the work of (Campbell et al., 2024), we employ a conditional flow to linearly interpolate from a uniform prior to  $x_1^{(i)}$ . This requires that the probability vector satisfies  $s_1 = \text{onehot}(c_i)$  and  $s_0 = (\frac{1}{4}, \dots, \frac{1}{4})$ . The conditional flow of the probability vector is then given by:

$$s_t = ts_1 + (1-t)s_0, \quad (11)$$

and the corresponding conditional vector field is:

$$u_t(s|s_0, s_1) = s_1 - s_0. \quad (12)$$

We use the neural network  $\mathbf{v}_{\theta}(\cdot)$  to predict the vector field of nucleotide types. The network’s training objective is optimized by minimizing the following loss:



$$\mathcal{L}_{\text{type}} = \mathbb{E}_{t \sim \mathcal{U}(0,1), p_1(s_1), p_0(s_0), p_t(s_t | s_1, s_0)} \sum_{i=1}^{N_t} \text{CE}(s_t^{(i)} + (1-t)v_\theta(s_t^{(i)}), s_1^{(i)}), \quad (13)$$

where  $\text{CE}(\cdot)$  is the cross-entropy function. This loss directly measures the difference between the true probability distribution and the inferred distribution for the RNA sequence.

#### 4.5. Distance-Aware Ligand Guided RNA Generation

While the preceding sections detailed the unconditional RNA generation through the synergistic flow matching, it is still necessary to incorporate ligand information during the training and sampling phases to guide the model toward producing RNA with specific ligand binding affinity. Therefore, we introduce a hierarchical RNA-ligand interaction module that explicitly incorporates ligand information into the RNA generation process.

Given a ligand  $\mathcal{M} = \{(a^{(j)}, b^{(j)})\}_{j=1}^{N_m}$ , a two-stage distance-aware structure refinement process is designed to implicitly optimize the binding free energy by modeling 3D RNA-ligand interactions. In the first stage, a multi-layer perceptron (MLP) is employed to learn the embedding  $h_a$  for atoms in the ligand. Subsequently, an invariant point attention (IPA) module predicts the initial RNA structural frame  $\hat{F}_1 = \{(\hat{x}_1^{(i)}, \hat{r}_1^{(i)})\}_{i=1}^{N_t}$  without considering ligand interaction. Next, We compute the spatial interaction feature  $h_b$  between the  $i$ -th RNA backbone atom ( $i \in [1, N_t]$ ) and the  $j$ -th ligand atom ( $j \in [1, N_m]$ ) as:

$$h_b = \exp\left(-\gamma \|\hat{x}_1^{(i)} - b^{(j)}\|^2\right), \quad (14)$$

where  $\gamma$  is a scaling factor controlling the spatial sensitivity. In the second stage, the IPA module refines the structure using  $h_a$  and  $h_b$ , yielding the post-interaction RNA frame:

$$\tilde{F}_1 = \text{IPA}(\hat{F}_1, h_a, h_b). \quad (15)$$

This two-stage process produces a refined RNA structure conditioned on the specific ligand, enabling conditional flow matching optimization under ligand constraints.

#### 4.6. Training and Inference.

**Training.** To fully leverage ligand information as conditional inputs, we incorporate the entire RNA-ligand complex as input. Specifically, we sample  $x_t$ ,  $r_t$ , and  $c_t$  alongside the ligand information through the defined conditional probability paths. Consequently, the complete binding complex at time  $t$  serves as input to the vector field  $v_t(\cdot)$ , represented as  $v_t(\cdot | \mathcal{T} \cup \mathcal{M}) = v_t(\cdot | \mathcal{C}_t)$ . Thus, the overall training loss can be expressed as:

$$\mathcal{L}_{\text{total}} = \mathbb{E}_c(\mathcal{L}_{\text{trans}} + \mathcal{L}_{\text{rot}} + \mathcal{L}_{\text{torsion}} + \mathcal{L}_{\text{type}}). \quad (16)$$

---

#### Algorithm 1 RiboFlow: Inference

---

**Input:** Ligand structure  $\mathcal{M}$ , Sampling steps  $T$ , Initial RNA structure  $\mathcal{T}_0$  with length  $N$ , Trained model  $v_\theta$   
Initialize:  $\text{steps} \leftarrow 0$ ,  $t \leftarrow 0$ ,  $\Delta t \leftarrow 1/T$   
Initialize: complex  $\mathcal{C}_0$  with RNA  $\mathcal{T}_0$  and ligand  $\mathcal{M}$   
**while**  $\text{steps} < T$  **do**  
 $x_{t+\Delta t}^{(i)} \leftarrow x_t^{(i)} + v_\theta(x_t^{(i)}, t; \mathcal{C}_t)\Delta t$   
 $r_{t+\Delta t}^{(i)} \leftarrow r_t^{(i)} \exp\left(v_\theta(r_t^{(i)}, t; \mathcal{C}_t)\Delta t\right)$   
 $s_{t+\Delta t}^{(i)} \leftarrow \text{norm}(s_t^{(i)} + v_\theta(s_t^{(i)}, t; \mathcal{C}_t)\Delta t)$   
Sample nucleotide type:  $c_{t+\Delta t}^{(i)} \sim s_{t+\Delta t}^{(i)}$   
 $t \leftarrow t + \Delta t$ ,  $\text{steps} \leftarrow \text{steps} + 1$   
**end while**  
Calculate:  $\hat{\Phi}_1^{(i)} \leftarrow v_\phi(\hat{x}_1^{(i)}, \hat{r}_1^{(i)})$   
**Return:** Final complex  $\mathcal{C}_1$

---

At this point, the loss about translation can be expanded as:

$$\mathcal{L}_{\text{trans}} = \mathbb{E}_{t \sim \mathcal{U}(0,1), p(x_1), p_0(x_0), p_t(x_t | x_0, x_1)} \|v_\theta(x; \mathcal{C}) - x_1^{(i)} + x_0^{(i)}\|_{\mathbb{R}^3}^2.$$

Similarly, the losses for rotation and nucleotide type can be formulated analogously. With these defined, the model is ready for training under specific ligand conditions.

**Inference.** The generation for an RNA of length  $N$  is initiated by creating a random point cloud as a structure frame and a random RNA sequence of the same length. Besides, the 3D structure of a ligand is incorporated as the conditional input. This noisy frame and sequence are then iteratively refined into a realistic RNA structure and sequence through the trained model  $v_\theta$  and an ODEsolver. The sampling process is detailed in the Algorithm 1.

## 5. Experiments

**Pretraining Dataset.** To establish foundational priors for RNA structural validity, we pre-train RiboFlow on RNA-solo<sup>1</sup> (Adamczyk et al., 2022), a curated database of single-stranded RNA 3D structures. We filter entries to those with resolution  $\leq 4$  Å (as of December 2024) and retain sequences between 30–200 nucleotides to balance structural diversity with computational feasibility, yielding 7,154 high-quality training samples. This length range reflects typical functional RNA motifs while accommodating GPU memory constraints. Single-stranded RNAs are prioritized to focus on unpaired regions critical for ligand binding.

**RNA-ligand Interaction Dataset.** We introduce RiboBind, the largest standardized dataset for RNA-small molecule interactions, addressing data scarcity in ligand-conditioned design. We discuss dataset construction and perform statistical analysis in the Appendix A.1. For sequences of

<sup>1</sup><https://rnasolo.cs.put.poznan.pl>

Table 1: Evaluation for Unconditional RNA Generation.

Method	%Validity( $\uparrow$ )	Diversity( $\uparrow$ )	Novelty( $\downarrow$ )
<b>RNA-FrameFlow</b>			
step_50	25.0	0.573	0.582
step_100	30.3	0.503	0.594
<b>RiboFlow-Structure</b>			
step_50	26.3	<b>0.577</b>	0.562
step_100	30.7	0.530	0.546
<b>RiboFlow-Codesign</b>			
step_50	<b>37.0</b>	0.550	<b>0.540</b>
step_100	34.3	0.545	0.577

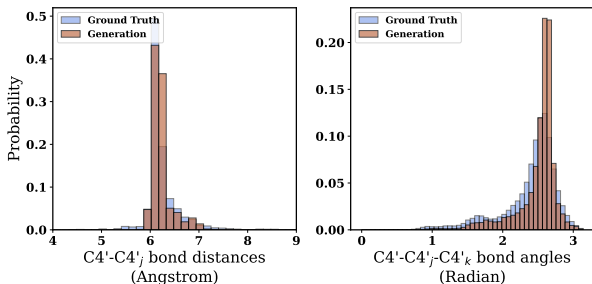


Figure 3: The probability distribution statistics of generated data and real data in bond distances and bond angles.

more than 200 nucleotides, we perform *dynamic cropping* and truncate regions distal to the ligand-binding pocket, preserving interaction sites while maximizing data utility (details discussed in Appendix A.2). The dataset after data augmentation contains 4,445 RNA-ligand pairs.

**Dataset Splits.** To evaluate generalization, we partition RiboBind into: **(1) Standard Evaluation Set:** Contains 66 RNA-ligand pairs derived from the 20 most frequent ligands. RNA sequences are clustered at 50% sequence similarity using MMseqs2 (Steinegger & Söding, 2017), with cluster centroids selected to ensure structural diversity. **(2) Few-shot Set:** Includes 15 pairs with ligands appearing only once in training, testing low-data generalization. Both sets exclude training ligands to prevent leakage.

**Evaluation Metrics.** We evaluate our experiment using metrics for both generation quality and binding capability. *For generation quality*, we focus on four metrics: **Validity (val.)**, assessed by inverse-folding each generated backbone with gRNAde (Joshi et al., 2024) and predicting its structure using RhoFold (Shen et al., 2024) with 8 generated sequences. The validity is determined by a self-consistency TM-score (scTM) between the predicted and original backbone at the C4' level, with scTM  $\geq 0.45$  indicating a valid backbone; **Diversity (div.)**, measured by the proportion of unique structural clusters (identified by qTMclust (Zhang et al., 2022)) among valid samples, Structures with a TM-score  $\geq 0.45$  are considered similar, reflecting the structural

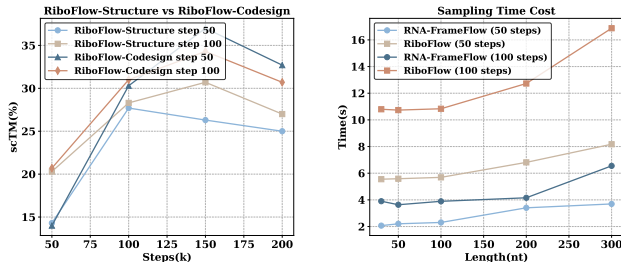


Figure 4: (Left): Performance of two pretraining tasks across different pre-training steps. (Right): Sampling time between RiboFlow (with ligand ARG) and RNA-FrameFlow (without ligand) for RNAs of varying lengths.

variability of generated samples; and **Novelty (nov.)**, evaluated using US-align (Zhang et al., 2022) to compare the structure of valid backbones to the training distribution, with higher novelty indicating greater structural divergence. **Sequence Recovery (SR.)**, quantified as the percentage of correctly recovered nucleotides in the co-designed sequence relative to the ground-truth RNA.

*For binding capability*, we assess the complex binding capability by four metrics: **VinaScore (vina.)**, the binding free energy (in *kcal/mol*) between RNA and ligand predicted by GNINA (Dunn et al., 2024), with lower values signifying stronger binding; **PoseScore (pose.)**, a measure of the ligand’s binding pose quality predicted by GNINA, and is defined as the proportion of binding pose probability exceeds the threshold of 0.6; **Affinity**, predicted binding affinity by GNINA, with higher values indicating stronger binding; and **AFScore (AF.)**, AlphaFold3’s overall prediction confidence for the complex, incorporating structural confidences (pTM and ipTM), clash penalties, and considerations for disordered regions, where higher scores are better.

**Baselines.** To the best of our knowledge, there is currently no RNA design model specifically targeting small molecules. RNAFlow (Nori & Jin, 2024) relies on RoseTTAFoldNA (Baek et al., 2024) to design RNA structures from predicted protein-RNA complex structures, which cannot predict RNA-ligand complex conformations. MMDiff (Morehead et al., 2023) is also limited to protein-RNA generation. Meanwhile, LigandMPNN (Dauparas et al., 2023) can only generate proteins for specific ligands. To this end, we choose RNA-FrameFlow (Anand et al., 2024) for comparison as it is a general RNA structure generation model, despite not being constrained by ligands. For further comparison, we also include a baseline where sequences are randomly generated and folded using RhoFold.

## 5.1. Unconditional RNA Generation

**Setup.** We evaluate the generative capabilities of models without small molecule information conditioned. Mean-

Table 2: Comparison of RNA generation under different conditions.

	VINA. (↓)		AFFINITY (↑)		%POSE. (↑)	%AF. (↑)	%VAL.(↑)	DIV.(↑)	NOV.(↓)
	TOP10	MEDIAN	TOP10	MEDIAN					
GENERATION GIVEN LIGAND STRUCTURE AND TRUE LENGTH									
RANDOM	-2.76	-2.55	2.34	2.31	4.20	3.11	-	-	-
RNA-FRAMEFLOW	-4.15	-4.01	3.12	3.02	59.6	17.4	22.5	0.288	0.584
RIBOFLOW	-4.25	-4.12	3.54	3.28	69.4	22.8	10.8	0.226	0.640
+ PRE	<b>-4.39</b>	<b>-4.31</b>	3.56	<u>3.34</u>	<u>71.8</u>	<u>48.4</u>	<b>30.8</b>	<u>0.354</u>	<b>0.514</b>
+ CROP	<u>-4.38</u>	<u>-4.27</u>	<u>3.59</u>	3.30	70.3	34.7	12.1	0.293	0.603
+ PRE + CROP	-4.30	-4.18	<b>3.61</b>	<b>3.35</b>	<b>78.5</b>	<b>50.1</b>	<u>24.2</u>	<b>0.376</b>	<u>0.534</u>
GENERATION GIVEN LIGAND STRUCTURE AND SAMPLING LENGTH									
RANDOM	-2.91	-2.82	2.41	2.24	5.24	5.25	-	-	-
RNA-FRAMEFLOW	-4.27	-4.15	3.32	3.14	55.7	22.7	22.7	0.545	0.574
RIBOFLOW	-4.61	-4.48	3.79	3.55	65.5	25.7	10.8	0.517	0.669
+ PRE	<b>-4.67</b>	<u>-4.55</u>	<u>3.92</u>	<b>3.70</b>	<u>73.6</u>	<u>51.2</u>	<b>35.8</b>	<u>0.575</u>	<b>0.519</b>
+ CROP	<u>-4.63</u>	<b>-4.56</b>	<b>3.94</b>	<u>3.66</u>	66.9	38.9	12.7	0.522	0.613
+ PRE + CROP	-4.58	-4.43	3.82	3.60	<b>74.6</b>	<b>54.8</b>	<u>25.6</u>	<b>0.589</b>	<u>0.527</u>
GENERATION GIVEN LIGAND SMILES AND SAMPLING LENGTH									
RANDOM	-3.32	-3.13	2.53	2.51	6.00	3.54	-	-	-
RNA-FRAMEFLOW	-4.51	-4.48	3.61	3.54	65.3	22.3	23.9	0.556	0.581
RIBOFLOW	-5.01	-4.82	4.21	3.97	62.3	15.4	11.2	0.522	0.656
+ PRE	<b>-5.12</b>	<b>-5.07</b>	<u>4.40</u>	<b>4.11</b>	72.6	<u>45.7</u>	<b>34.1</b>	<b>0.561</b>	<u>0.537</u>
+ CROP	<u>-5.10</u>	<u>-4.99</u>	4.29	4.02	66.7	27.9	12.3	0.546	0.609
+ PRE + CROP	-4.96	-4.84	4.31	4.03	<u>73.8</u>	39.8	<u>26.1</u>	0.559	0.540
RIBOFLOW-T	-5.07	-4.94	<b>4.42</b>	<u>4.05</u>	<b>75.1</b>	<b>46.2</b>	22.4	0.550	<b>0.524</b>

while, to validate the effectiveness of the co-design pre-training strategy proposed in the paper, we design two different pre-training tasks: (i) utilizing only the RNA structural backbone frames and torsion angle loss (RiboFlow-Structure), and (ii) incorporating nucleotide type loss simultaneously (RiboFlow-Codesign). For each model, we set the RNA generation length within the range of [50, 150], sampling at intervals of 20, and generate 50 samples for each length to thoroughly cover the model’s sampling space.

**Results.** The experimental results are shown in Table 1, with local structural metrics of RNA generated by the RiboFlow-Codesign depicted in Figure 3. Additionally, we provide a detailed comparison of model performance under different pre-training steps in Table S1. We can draw the following conclusions: (i) The validity of RNAs generated by RiboFlow-Codesign has shown significant improvement compared to the other baselines. (ii) Due to the addition of sequence feature constraints, the diversity of RNAs generated by the Codesign model has slightly decreased compared to RiboFlow-Structure. (iii) Increasing the sampling steps can enhance the validity of RNA structures to a certain extent but will reduce the diversity of the model. Besides, it can also be noted that the structures generated by RiboFlow-Codesign are close to the real structures in terms of bond lengths and torsion angles in Table 1, which further proves

Table 3: Sequence recovery and structural RMSD comparisons with ground-truth RNA using ligand-bound structures and true sequence lengths.

METHOD	%SR (↑)	RMSD (↓)
RANDOM	25.0	-
RNA-FRAMEFLOW	32.2	8.92
RIBOFLOW	37.9	9.66
+PRE	<b>47.4</b>	<b>5.94</b>
+CROP	40.6	<u>7.03</u>
+PRE+CROP	<u>43.8</u>	7.34

the effectiveness of the co-design pre-training strategy.

## 5.2. RNA Generation Guided by Ligand Structure

We evaluate the performance of models conditioned on ligand-bound structures and further examine the impact of incorporating the ground-truth RNA sequence length as a prompt. Hence, we design two protocols: (a) using the true RNA sequence length for generation, and (b) employing uniform sampling of RNA lengths within a predefined range. Both protocols are tested on the standard evaluation set. Additionally, we expand our analysis to include the few-shot evaluation set (detailed in the Appendix Table S2) to assess the model’s performance in low-resource scenarios.

**Setup.** We include three types of model variants in addition to the original model: (i) RiboFlow: The baseline model trained on the RiboBind; (ii) +CROP: Model trained on the RiboBind augmented with dynamic cropping strategy; (iii) +PRE: Model trained on the RiboBind using codesign pretrained weights; (iv) +PRE+CROP: Model trained on RiboBind augmented with dynamic cropping strategy using codesign pretrained weights. The ligand-bound structures are provided to models as guidance. For protocol (a), 50 RNAs of actual length are sampled for each RNA-ligand pair. As for protocol (b), the range is defined as [50,150], sampling at intervals of 20, and generated 50 samples for each length, resulting in a total of 300 RNAs. These candidate RNAs are subsequently evaluated based on their structural validity and binding capability with the ligand.

**Results.** We first analyze the experimental results provided with the ground-truth RNA lengths, as shown in Table 2 in the gray-shaded section and Table 3, with best results in bold and the second-best results underlined. Furthermore, we provide detailed experimental results for 24 randomly selected RNA-ligand pairs presented in Figures S7, showcasing the *vina* and *posescore* with actual values as reference. Several interesting conclusions can be summarized: (i) The diversity for all models are significantly lower than those observed in Table 1, which indicates that constraining the RNA length compresses the sequence sampling space, leading to a decrease in diversity; (ii) Models incorporating co-design pre-training strategy (PRE and PRE-CROP) demonstrate a substantial advantage in structural validity and binding capability. Besides, we can also observe that these two models also perform excellently in terms of sequence recovery rate and RMSD metrics in Table 3; (iii) Compared to the codesign-pretraining, there is no significant improvement in structural validity under the dynamic cropping strategy. This may be because the trimmed RNA fragments may not fold into the real RNA structure, thus the model cannot effectively learn the true structural distribution. However, data augmentation expands the training data, allowing the model to learn a more diverse set of RNA-ligand docking patterns and improve the designed RNA binding capability.

Subsequently, we analyze the experimental results when length is sampling from the pre-defined ranges in Table 2 highlighted in the blue-shaded section. Most experimental conclusions are similar to the previous ones, but due to the increase in the length sampling space, models can explore more potential binding patterns, and the results of all model variants on Vina, Affinity, and AFScore increase largely.

We conduct similar experiments on few-shot set, and experimental results can be referred to the Appendix B.3.

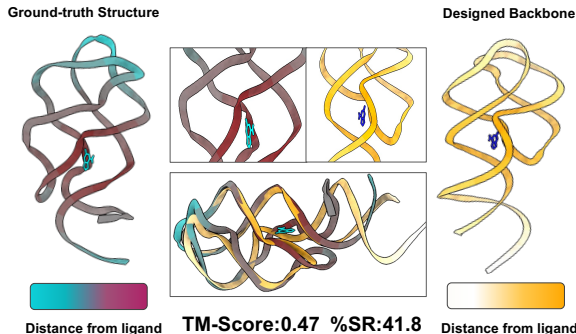


Figure 5: *De novo* design of an RNA corresponding to ligand A2F. Left: The ground-truth RNA-ligand complex (PDB ID: 3GOT). Right: RNA backbone designed by RiboFlow, with ligand docking by GNINA. The designed structure achieves a TM-score of 0.47 and a Sequence Recovery (SR) of 41.8% compared to the ground-truth complex.

### 5.3. RNA Generation Guided by Ligand SMILES

A common challenge in **real-world applications** is the lack of knowledge regarding the precise RNA length and its ligand-bound conformation. This section try to explore whether our model can successfully design small molecule RNA binders despite this significant limitation.

**Setup.** We employ RDKit to generate 3D ligand conformers from SMILES, with subsequent optimization using the MMFF force field (Tosco et al., 2014). RNA lengths are sampled at intervals of 20 within the range [50, 150], with 50 candidate structures generated per length. Moreover, we introduce RiboFlow-T, a variant that translates the coordinate system to the ligand centroid during the training of RiboFlow-PRE-CROP. This modification aims to minimize the impact of ligand spatial positioning on RNA-ligand complex modeling. The nucleotide structure frames are subsequently constructed relative to this transformed coordinates.

**Results.** The experimental results are shown in Table 2 highlighted in the pink-shaded section, which reveals the following insights: RiboFlow-T achieves the highest docking pose score, indicating that re-centering on the ligand’s centroid during training improves docking pattern reliability. However, this approach introduces inconsistencies with the RNA-centered coordinate system used during pretraining, reducing RNA structure validity.

We also leverage RiboFlow to *de novo* design RNA conditioned on ligand A2F and GNG, with the experimental results presented in the Figure 5 and Appendix B.4.

## 6. Conclusion

In this work, we propose RiboFlow, the first generative model designed for ligand-specific RNA generation. By



leveraging RNA backbone frames, torsion angles, and sequence features via conditional flow matching, RiboFlow can effectively capture the conformational flexibility of RNA while improving structural validity through sequence constraints. Additionally, RiboFlow models the 3D RNA-ligand interaction to optimize RNA generation, implicitly enhancing its binding affinity. Extensive experiments demonstrate the ability of RiboFlow to generate RNA structures with both high validity and target-specific affinity.

## Impact Statement

Driven by the rapid advancement of artificial intelligence, the field of drug discovery is undergoing profound transformations. AI-based drug discovery offers the potential to significantly benefit humanity and enhance the expected quality of life. The remarkable success of mRNA vaccines during the COVID-19 pandemic, which saved countless lives, highlighted the importance of RNA engineering. Inspired by the broad application scenarios of RNA, we present RiboFlow, which, to the best of our knowledge, is the first deep generative model for the *de novo* design of RNA that targets specific molecules. We hope that RiboFlow can bring opportunities for the flourishing development of RNA therapeutic drugs and provide more research inspiration for pharmacologists and medical experts. Therefore, we hope that this important scientific contribution will receive the support of reviewers and the review committee.

## References

- Abramson, J., Adler, J., Dunger, J., Evans, R., et al. Accurate structure prediction of biomolecular interactions with alphafold3. *Nature*, pp. 493–500, 2024.
- Adamczyk, B., Antczak, M., and Szachniuk, M. Rnasolo: a repository of cleaned pdb-derived rna 3d structures. *Bioinformatics*, 38(14):3668–3670, 2022.
- Anand, R., Joshi, C. K., Morehead, A., Jamasb, A. R., Harris, C., Mathis, S., Didi, K., Hooi, B., and Liò, P. Rna-frameflow: Flow matching for de novo 3d rna backbone design. *arXiv preprint arXiv:2406.13839*, 2024.
- Baek, M., McHugh, R., Anishchenko, I., Jiang, H., Baker, D., and DiMaio, F. Accurate prediction of protein–nucleic acid complexes using rosettafoldna. *Nature methods*, 21(1):117–121, 2024.
- Bose, J., Akhound-Sadegh, T., Huguet, G., FATRAS, K., Rector-Brooks, J., Liu, C.-H., Nica, A. C., Korablyov, M., Bronstein, M. M., and Tong, A. Se (3)-stochastic flow matching for protein backbone generation. In *The Twelfth International Conference on Learning Representations*, 2024.
- Campbell, A., Yim, J., Barzilay, R., Rainforth, T., and Jaakkola, T. Generative flows on discrete state-spaces: Enabling multimodal flows with applications to protein co-design. *arXiv preprint arXiv:2402.04997*, 2024.
- Cao, X., Zhang, Y., Ding, Y., and Wan, Y. Identification of rna structures and their roles in rna functions. *Nature Reviews Molecular Cell Biology*, pp. 1–18, 2024.
- Churkin, A., Retwitzer, M. D., Reinharz, V., Ponty, Y., Wald-ispühl, J., and Barash, D. Design of rnas: comparing programs for inverse rna folding. *Briefings in bioinformatics*, 19(2):350–358, 2018.
- Dao, Q., Phung, H., Nguyen, B., and Tran, A. Flow matching in latent space. *arXiv preprint arXiv:2307.08698*, 2023.
- Dauparas, J., Lee, G. R., Pecoraro, R., An, L., Anishchenko, I., Glasscock, C., and Baker, D. Atomic context-conditioned protein sequence design using ligandmpnn. *Biorxiv*, pp. 2023–12, 2023.
- Disney, J. L., Yang, X., Gibaut, Q. M., Tong, Y., Batey, R. T., and Disney, M. D. Targeting rna structures with small molecules. *Nature Reviews Drug Discovery*, 21(10):736–762, 2022.
- Dotu, I., Garcia-Martin, J. A., Slinger, B. L., Mechery, V., Meyer, M. M., and Clote, P. Complete rna inverse folding: computational design of functional hammerhead ribozymes. *Nucleic acids research*, 42(18):11752–11762, 2014.
- Dunn, I., Pirhadi, S., Wang, Y., Ravindran, S., Concepcion, C., and Koes, D. R. Cache challenge# 1: Docking with gnina is all you need. *Journal of Chemical Information and Modeling*, 2024.
- Esser, P., Kulal, S., Blattmann, A., Entezari, R., Müller, J., Saini, H., Levi, Y., Lorenz, D., Sauer, A., Boesel, F., et al. Scaling rectified flow transformers for high-resolution image synthesis. In *Forty-first International Conference on Machine Learning*, 2024.
- Falese, J. P., Donlic, A., and Hargrove, A. E. Targeting rna with small molecules: from fundamental principles towards the clinic. *Chemical Society Reviews*, 50(4):2224–2243, 2021.
- Gat, I., Remez, T., Shaul, N., Kreuk, F., Chen, R. T., Synnaeve, G., Adi, Y., and Lipman, Y. Discrete flow matching. *arXiv preprint arXiv:2407.15595*, 2024.
- Gelbin, A., Schneider, B., Clowney, L., Hsieh, S.-H., Olson, W. K., and Berman, H. M. Geometric parameters in nucleic acids: sugar and phosphate constituents. *Journal of the American Chemical Society*, 118(3):519–529, 1996.

- Goodfellow, I., Pouget-Abadie, J., Mirza, M., Xu, B., Warde-Farley, D., Ozair, S., Courville, A., and Bengio, Y. Generative adversarial nets. *Advances in neural information processing systems*, 27, 2014.
- He, K., Zhang, X., Ren, S., and Sun, J. Deep residual learning for image recognition. In *Proceedings of the IEEE conference on computer vision and pattern recognition*, pp. 770–778, 2016.
- Ho, J., Jain, A., and Abbeel, P. Denoising diffusion probabilistic models. *Advances in neural information processing systems*, 33:6840–6851, 2020.
- Hua, C., Liu, Y., Zhang, D., Zhang, O., Luan, S., Yang, K. K., Wolf, G., Precup, D., and Zheng, S. Enzymeflow: Generating reaction-specific enzyme catalytic pockets through flow matching and co-evolutionary dynamics. *arXiv preprint arXiv:2410.00327*, 2024.
- Huang, H., Lin, Z., He, D., Hong, L., and Li, Y. Ribodiffusion: tertiary structure-based rna inverse folding with generative diffusion models. *Bioinformatics*, 40 (Supplement\_1):i347–i356, 2024.
- Huguet, G., Vuckovic, J., Fatras, K., Thibodeau-Laufer, E., Lemos, P., Islam, R., Liu, C.-H., Rector-Brooks, J., Akhound-Sadegh, T., Bronstein, M., et al. Sequence-augmented se (3)-flow matching for conditional protein backbone generation. *Advances in neural information processing systems*, 2024.
- Joshi, C. K., Jamasb, A. R., Viñas, R., Harris, C., Mathis, S., Morehead, A., Anand, R., and Liò, P. gnnade: Geometric deep learning for 3d rna inverse design. *bioRxiv*, 2024.
- Jumper, J., Evans, R., Pritzel, A., Green, T., Figurnov, M., Ronneberger, O., Tunyasuvunakool, K., Bates, R., Žídek, A., Potapenko, A., et al. Highly accurate protein structure prediction with alphafold. *nature*, 596(7873):583–589, 2021.
- Kingma, D. P. Auto-encoding variational bayes. In *The Eleventh International Conference on Learning Representations*, 2014.
- Lin, H., Zhang, O., Zhao, H., Jiang, D., Wu, L., Liu, Z., Huang, Y., and Li, S. Z. Ppflow: Target-aware peptide design with torsional flow matching. In *Forty-first International Conference on Machine Learning*, 2024.
- Lipman, Y., Chen, R. T., Ben-Hamu, H., Nickel, M., and Le, M. Flow matching for generative modeling. In *The Eleventh International Conference on Learning Representations*, 2023.
- Liu, X., Gong, C., et al. Flow straight and fast: Learning to generate and transfer data with rectified flow. In *The Eleventh International Conference on Learning Representations*, 2023.
- Morehead, A., Ruffolo, J., Bhatnagar, A., and Madani, A. Towards joint sequence-structure generation of nucleic acid and protein complexes with se (3)-discrete diffusion. *arXiv preprint arXiv:2401.06151*, 2023.
- Nori, D. and Jin, W. Rnaflow: Rna structure & sequence design via inverse folding-based flow matching. *arXiv preprint arXiv:2405.18768*, 2024.
- Panei, F. P., Torchet, R., Menager, H., Gkeka, P., and Bonomi, M. Hariboss: a curated database of rna-small molecules structures to aid rational drug design. *Bioinformatics*, 38(17):4185–4193, 2022.
- Runge, F., Stoll, D., Falkner, S., and Hutter, F. Learning to design rna. In *International Conference on Learning Representations*, 2019.
- Shen, T., Hu, Z., Sun, S., Liu, D., Wong, F., Wang, J., Chen, J., Wang, Y., Hong, L., Xiao, J., et al. Accurate rna 3d structure prediction using a language model-based deep learning approach. *Nature Methods*, pp. 1–12, 2024.
- Steinegger, M. and Söding, J. Mmseqs2 enables sensitive protein sequence searching for the analysis of massive data sets. *Nature biotechnology*, 35(11):1026–1028, 2017.
- Sun, L.-Z., Jiang, Y., Zhou, Y., and Chen, S.-J. Rldock: a new method for predicting rna–ligand interactions. *Journal of chemical theory and computation*, 16(11):7173–7183, 2020.
- Tan, C., Zhang, Y., Gao, Z., Hu, B., Li, S., Liu, Z., and Li, S. Z. Rdesign: Hierarchical data-efficient representation learning for tertiary structure-based rna design. In *The Twelfth International Conference on Learning Representations*, 2024.
- Tong, A., FATRAS, K., Malkin, N., Huguet, G., Zhang, Y., Rector-Brooks, J., Wolf, G., and Bengio, Y. Improving and generalizing flow-based generative models with minibatch optimal transport. *Transactions on Machine Learning Research*, 2024.
- Tosco, P., Stiefl, N., and Landrum, G. Bringing the mmff force field to the rdkit: implementation and validation. *Journal of cheminformatics*, 6:1–4, 2014.
- Wang, Z., Ji, Y., Tian, J., and Zheng, S. Retrieval augmented diffusion model for structure-informed antibody design and optimization. *arXiv preprint arXiv:2410.15040*, 2024.

- Wilson, T. J. and Lilley, D. M. The potential versatility of rna catalysis. *Wiley Interdisciplinary Reviews: RNA*, 12(5):e1651, 2021.
- Wong, F., He, D., Krishnan, A., Hong, L., Wang, A. Z., Wang, J., Hu, Z., Omori, S., Li, A., Rao, J., et al. Deep generative design of rna aptamers using structural predictions. *Nature Computational Science*, pp. 1–11, 2024.
- Yang, X., Yoshizoe, K., Taneda, A., and Tsuda, K. Rna inverse folding using monte carlo tree search. *BMC bioinformatics*, 18:1–12, 2017.
- Yim, J., Campbell, A., Foong, A. Y., Gastegger, M., Jiménez-Luna, J., Lewis, S., Satorras, V. G., Veeling, B. S., Barzilay, R., Jaakkola, T., et al. Fast protein backbone generation with se (3) flow matching. *arXiv preprint arXiv:2310.05297*, 2023.
- Zambaldi, V., La, D., Chu, A. E., Patani, H., Danson, A. E., Kwan, T. O., Frerix, T., Schneider, R. G., Saxton, D., Thillaisundaram, A., et al. De novo design of high-affinity protein binders with alphaproteo. *arXiv preprint arXiv:2409.08022*, 2024.
- Zhang, C., Shine, M., Pyle, A. M., and Zhang, Y. Us-align: universal structure alignments of proteins, nucleic acids, and macromolecular complexes. *Nature methods*, 19(9): 1109–1115, 2022.
- Zhang, Z., Wang, M., and Liu, Q. Flexsbdd: Structure-based drug design with flexible protein modeling. In *The Thirty-eighth Annual Conference on Neural Information Processing Systems*, 2024.

## A. Dataset

### A.1. Dataset Preparation

In this work, we propose RiboBind, the largest RNA-ligand binding dataset to date. RiboBind contains all RNA-small molecule interaction information stored in the RCSB PDB database up to December 2024. The data preparation workflow is described in detail as follows.

(i) *Data collection.* We obtain raw structural data in CIF format from the RCSB PDB database using the advanced search query builder, which supports custom filtering based on specific structural attributes. The search is restricted to structures containing at least one RNA polymer chain and one ligand instance. These criteria are defined using the following query settings: Structure Attributes  $\rightarrow$  Number of Distinct RNA Entities  $\geq 1$  and Structure Attributes  $\rightarrow$  Total Number of Non-polymer Instances  $\geq 1$ . This step serves as the initial data collection phase.

(ii) *Ligand filtering.* We adopt a portion of the ligand selection criteria from the HairBoss database (Panei et al., 2022), while relaxing certain rigid druggability restrictions, aiming to balance ligand diversity and effective identification. Specifically, the following rules are applied during our workflow: (1) the molecular weight of the ligand must fall within the range of 100-1000 Daltons, and (2) the ligand must not be a solvent molecule or a metal ion. Consequently, we expand the original ligand library beyond the 311 ligand classes used in HairBoss by incorporating an additional 237 ligand classes, resulting in a total of 548 unique ligand classes.

(iii) *RNA-ligand interactions determination.* For structures containing valid ligands, RNA-ligand interactions are identified by calculating the minimum distance between any ligand atom and any RNA atom. If the minimum distance is less than or equal to 5 Å, the ligand is considered to interact with the RNA. Using this criterion, we extract RNA chains and their corresponding interacting ligands from the crystal structures to construct RNA-ligand complexes. Each complex is subsequently decomposed into individual RNA-ligand pairs, where each pair comprises a single RNA chain and its interacting ligand.

(iv) *Redundancy reduction.* To reduce redundancy and improve dataset quality, we employ MMseqs2 (Steinegger & Söding, 2017) to cluster RNA sequences at a 90% sequence identity threshold. Notably, RNA sequences within the same cluster but bound to different ligands are still treated as distinct RNA-ligand pairs.

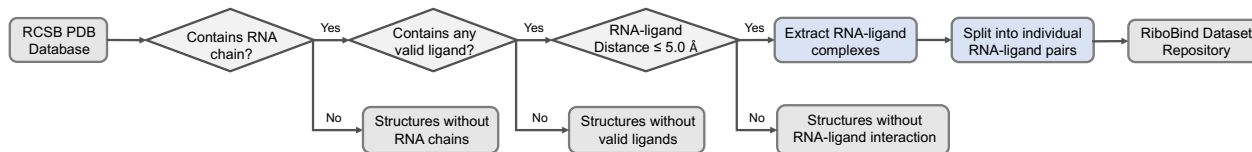


Figure S1: The collection pipeline of RiboBind dataset.

Through this comprehensive pipeline, we construct the RiboBind dataset, offering a substantially larger and more diverse collection of RNA-small molecule interactions compared to existing datasets. The final RiboBind dataset includes 1,591 RNA-ligand complexes and 3,012 RNA-ligand pairs. In comparison, as of December 2024, the publicly accessible HairBoss dataset comprises only 862 RNA-ligand complexes and 1,471 RNA-ligand pairs. This notable increase in both scale and diversity highlights the value of RiboBind as a robust resource for RNA-small molecule interaction studies.

### A.2. Data Augmentation

To prevent graphics memory overflow during experiments, the RNA length is restricted to the range of 30-200 nucleotides during training. However, the original RiboBind dataset contains a limited number of samples within this length range, which is insufficient to satisfy the large-scale data requirements of deep generative models. To address this challenge, we introduce a data augmentation strategy called *dynamic cropping*, designed to fully leverage existing data resources by modifying RNA sequences longer than 200 nucleotides.

In order to ensure that the cropped RNA sequences retain interactions with small molecules, the cropping strategy is informed by interaction data from existing datasets. Specifically, we select RNA bases involved in interactions with the



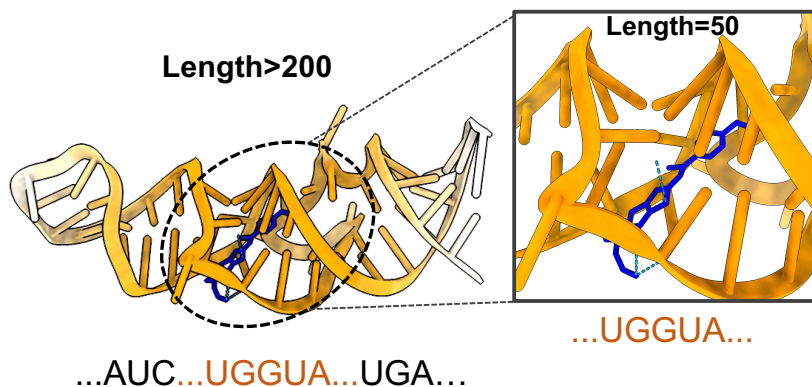


Figure S2: An example of RNA dynamic cropping. Based on a selected nucleotide, we randomly select a cropping length within the range of 30 to 200 to obtain the trimmed RNA-ligand pair for amplifying the existing data.

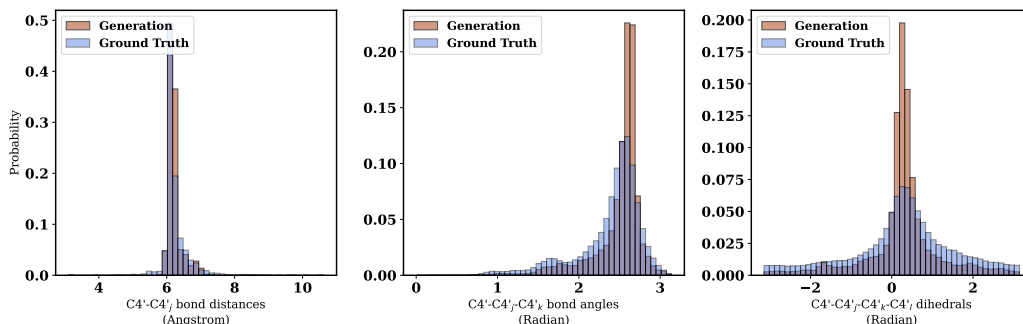


Figure S3: Comparison of probability distribution histograms of nucleotide bond distances, bond angles, and torsion angles between the generated RNA and the real RNA structure.

small molecules as candidate bases. By calculating the total interaction counts between each base and every atom in the small molecules, we can identify the top three bases with the highest interaction frequencies as cropping centers. The cropping length is randomly sampled within the range of 30–200 nucleotides. Using the selected base as the center, the RNA sequence is cropped symmetrically, with half the total length taken from both upstream and downstream of the base, forming the final RNA-ligand pair. This approach ensures that the cropped RNA sequences retain critical interaction information for downstream tasks.

Through this dynamic cropping strategy, the number of qualified RNA-ligand pairs in the original RiboBind dataset increased from 1,061 to 4,445, significantly expanding the available training data.

## B. More Results and Analysis

### B.1. The Impact of Pre-training Steps on RNA Generation

To fully demonstrate the impact of different pre-training steps on RNA generation, we comprehensively show the changes in model performance under various pre-training steps. We additionally introduced the scRMSD metric to evaluate the performance changes. During the pre-training stage, a batch size of 32 is selected, utilizing 4 A100 80GB accelerator cards, completing 200K pre-training steps in nearly 20 hours. The experimental results are shown in Table S1.

Table S1: Detailed results of unconditional generation under different pre-training steps.

METHOD	%SCTM(↑)	%SCRSMD(↑)	DIVERSITY(↑)	NOVELTY(↓)
RNAFRAME-FLOW				
STEP_50	25.0	24.7	<b>0.573</b>	<b>0.582</b>
STEP_100	<b>30.3</b>	<b>28.3</b>	0.503	0.594
RIBOFLOW-STRUCTURE				
50K_STEP_50	14.3	16.0	<b>0.733</b>	0.677
50K_STEP_100	20.3	19.3	0.703	0.670
100K_STEP_50	27.7	26.7	0.550	0.597
100K_STEP_100	28.3	<b>27.0</b>	0.547	0.586
150K_STEP_50	26.3	22.7	0.577	0.562
150K_STEP_100	<b>30.7</b>	24.8	0.530	<b>0.546</b>
200K_STEP_50	25.0	22.3	0.590	0.553
200K_STEP_100	27.0	24.3	0.537	0.559
RIBOFLOW-CODESIGN				
50K_STEP_50	14.0	21.7	<b>0.710</b>	0.685
50K_STEP_100	20.7	23.3	0.643	0.511
100K_STEP_50	30.3	29.0	0.583	0.589
100K_STEP_100	31.0	27.3	0.620	0.574
150K_STEP_50	<b>37.0</b>	<b>31.3</b>	0.550	<b>0.540</b>
150K_STEP_100	34.3	30.7	0.545	0.577
200K_STEP_50	32.7	26.7	0.520	0.581
200K_STEP_100	30.7	27.0	0.493	0.606

## B.2. The Local Structure of RNA Analysis

To demonstrate the validity of the generated RNA structures, we conduct a detailed comparison between the RNA structures generated by RiboFlow-Codesign within the [50,150] range and the actual RNA structure distributions. We primarily illustrate histograms of the probability distributions for the bond distances between nucleotides, the bond angles between nucleotide triplets, and the torsion angles, as shown in Figure S3. It can be observed that the structures of the RNA we generated are similar in distribution to those of real RNA, capable of reproducing the characteristics of these local structures.

## B.3. Experimental Results on Few-shot Set

Following the experimental setup of Section 5.2, we conduct similar experiments on the few-shot set, with the experimental results as shown in Table S2. It can be observed that despite the model being exposed to only a small amount of sample information during training, it still demonstrated excellent performance. In addition, we have also presented the detailed results of vina and pose scores for these fifteen RNA-ligand pairs in the Figure S8, fully demonstrating the experimental performance of different model variants.

## B.4. Using RiboFlow for *De Novo* RNA Design

In this section, we aim to validate RiboFlow’s capability in designing *de novo* high-affinity RNAs for specific ligand targets. As a case study, we explore two design scenarios: one where the actual RNA length and small molecule binding structure (ligand A2F<sup>2</sup>) are provided, and another where neither the RNA length nor the binding structure (ligand GNG<sup>3</sup>) is given.

**Pipeline.** For ligand A2F. We employ RiboFlow to generate RNA sequences of length 67, which are then docked against A2F ligand-bound conformers using GNINA. A specific RNA candidate is selected based on a composite score integrating Vina and ligand pose scores. The corresponding ground-truth RNA sequence and the designed RNA sequence are presented in the results.

For ligand GNG. We first leverage RiboFlow to generate RNAs ranging from 50 to 150 nucleotides in length. These RNA

<sup>2</sup><https://www.rcsb.org/ligand/A2F>

<sup>3</sup><https://www.rcsb.org/ligand/GNG>

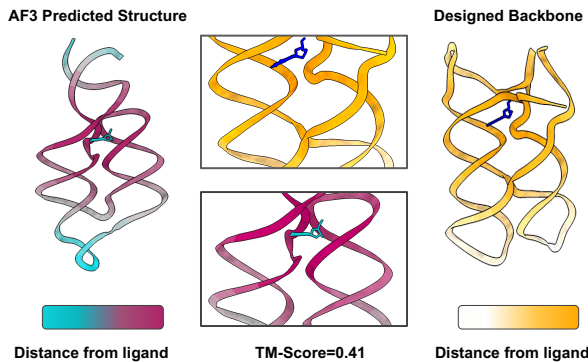


Figure S4: *De novo* design of a 90-nucleotide RNA corresponding to the ligand GNG with a molecular weight of 267.2 Da. The RNA-ligand complex structure is predicted by AlphaFold3, whereas another is generated by RiboFlow and docking using GNINA. The AlphaFold3-predicted complex structure exhibits a TM-score of 0.41 and an RMSD of 3.82 Å compared to the RiboFlow-designed RNA backbone, demonstrating the validity of the designed RNA.

sequences are then docked against GNG conformers, generated by RDKit, using GNINA. A 90-nucleotide RNA candidate is selected based on a composite score that integrates vina and ligand pose scores. To validate this candidate, gRNAde is applied to determine its corresponding sequence, and AlphaFold3 predicts the structure of the resulting RNA-GNG complex.

**Case Analysis.** For ligand A2F. The ground-truth RNA-ligand complex used in our study has a PDB ID of 3GOT. The TM-score between our designed RNA and the native RNA is 0.47, with a sequence recovery rate of 41.8%, as shown in Figure 5. Below, we provide both the designed RNA sequence and the corresponding native RNA sequence for comparison:

```
>Ground-truth RNA Sequence (3GOT)
GGACAUAAUAAUCGCGUGGAUAUGGCACGCAAGUUUCUACCGGGCACCGUAAAUGUCCGAUUAUGUCC
>Designed RNA Sequence
CGGUGGGAAGGGGUGAGGCCAGGCUAUACCUGGCGCAACGUCUCACCUUUAUAGGGCAAGCCUUGCC
```

For ligand GNG. The AlphaFold3-predicted complex structure exhibits a TM-score of 0.41 and an RMSD of 3.82 Å compared to the RiboFlow-designed RNA backbone, demonstrating the validity of the designed RNA. Furthermore, as illustrated in Figure S4, a high consistency is observed between the GNINA-predicted binding pocket and the AlphaFold3-predicted binding region. These findings provide strong support for RiboFlow’s potential to facilitate the design of RNAs with high binding affinity.

## C. Flow Matching

Flow Matching (FM) (Lipman et al., 2023) is a method designed to reduce the simulation required for learning Continuous Normalizing Flows (CNFs), which is a class of deep generative models that generate data by integrating an ordinary differential equation (ODE) over a learned vector field. In this section, we will provide a concise overview of the flow matching approach.

A continuous normalizing flow  $\phi_t(\cdot) : \mathcal{M} \rightarrow \mathcal{M}$  on a manifold  $\mathcal{M}$  is defined as the solution to a time-dependent vector field  $v_t(x) \in \mathcal{T}x\mathcal{M}$ , where  $\mathcal{T}x\mathcal{M}$  represents the tangent space of  $\mathcal{M}$  at  $x \in \mathcal{M}$ :

$$\frac{d}{dt}\phi_t(x) = v_t(\phi_t(x)), \quad \phi_0(x) = x. \quad (17)$$

The parameter  $t$  evolves within  $[0, 1]$ , and the flow transforms a simple prior density  $p_0$  into the data distribution  $p_1$  via the push-forward equation  $p_t = [\phi_t]_* p_0$ . The density of  $p_t$  is given by:

$$p_t(x) = [\phi_t]_* p_0(x) = p_0(\phi_t^{-1}(x)) e^{-\int_0^t \text{div}(v_s)(x_s) ds}. \quad (18)$$

The sequence of distributions  $p_t : t \in [0, 1]$  is referred to as the *probability path*. While the vector field  $v_t$  that generates a specific  $p_t$  is generally intractable, it can be approximated efficiently by expressing the target probability path as a mixture of

Table S2: Comparison of model performance on the few-shot evaluation set. The best results are highlighted in bold, while the second-best results are underlined. The table presents two experimental results: one based on a fixed RNA length and ligand-bound structure, and another based on ligand-bound structures with RNA length sampling. Colored boxes denote different experimental setups.

	VINA. (↓)		AFFINITY (↑)		%POSE. (↑)	AF. (↑)	%VAL.(↑)	DIV.(↑)	NOV.(↓)
	TOP10	MEDIAN	TOP10	MEDIAN					
GENERATION WITH GIVEN RNA LENGTH AND LIGAND CONFORMATION									
RANDOM	-2.16	-2.03	2.89	2.72	5.10	7.11	-	-	-
RNA-FRAMEFLOW	-3.95	-3.88	3.28	3.11	52.2	16.4	20.3	0.279	0.570
RIBOFLOW	<u>-4.63</u>	-4.49	3.68	3.55	67.2	22.8	9.68	0.216	0.645
+ PRE	<b>-4.74</b>	<b>-4.63</b>	<u>4.06</u>	<b>3.82</b>	<u>76.0</u>	<u>47.1</u>	<b>32.4</b>	<u>0.310</u>	<u>0.534</u>
+ CROP	-4.56	<u>-4.51</u>	<b>4.08</b>	<u>3.81</u>	73.3	25.6	18.1	0.257	0.623
+ PRE + CROP	-4.47	-4.41	4.05	3.79	<b>78.7</b>	<b>49.9</b>	<u>25.9</u>	<b>0.331</b>	<b>0.527</b>
GENERATION WITH GIVEN RNA LENGTH AND LIGAND CONFORMATION									
RANDOM	-2.23	-2.15	3.09	2.93	7.00	8.84	-	-	-
RNA-FRAMEFLOW	-4.35	-4.01	3.31	3.16	55.4	19.1	22.0	0.521	0.580
RIBOFLOW	-4.87	-4.66	3.90	3.78	70.4	24.1	10.2	0.529	0.664
+ PRE	<b>-5.04</b>	<b>-4.89</b>	<u>4.26</u>	<b>4.13</b>	<u>73.8</u>	<u>48.6</u>	<b>35.7</b>	<u>0.572</u>	<b>0.520</b>
+ CROP	-4.91	-4.75	<b>4.28</b>	4.06	72.0	32.4	17.4	0.535	0.622
+ PRE + CROP	<u>-4.96</u>	<u>-4.82</u>	4.21	<u>4.11</u>	<b>76.2</b>	<b>51.3</b>	<u>26.2</u>	<b>0.577</b>	<u>0.539</u>

simpler *conditional* probability paths,  $p_t(x|x_1)$ . These conditional paths satisfy  $p_0(x|x_1) = p_0(x)$  and  $p_1(x|x_1) \approx \delta(x - x_1)$ . The unconditional probability path  $p_t$  can then be recovered as the average of the conditional paths with respect to the data distribution:  $p_t(x) = \int p_t(x|x_1)p_1(x_1)dx_1$ .

To describe this further, let  $u_t(x|x_1) \in \mathcal{T}x\mathcal{M}$  denote the *conditional vector field* generating the conditional probability path  $p_t(x|x_1)$ . Flow matching builds on the insight that the unconditional vector field  $v_t$  can be learned by aligning it with the conditional vector field  $u_t(x|x_1)$  using the following objective:

$$\mathcal{L}_{\text{CFM}} := \mathbb{E}_{t, p_1(x_1), p_t(x|x_1)} [\|v_t(x) - u_t(x|x_1)\|_g^2], \quad (19)$$

where  $t \sim \mathcal{U}([0, 1])$ ,  $x_1 \sim p_1(x_1)$ ,  $x \sim p_t(x|x_1)$ , and  $\|\cdot\|_g^2$  represents the norm induced by the Riemannian metric  $g$ .

The objective can be reparameterized through the conditional flow,  $x_t = \psi_t(x_0|x_1)$ , where  $\psi_t$  satisfies  $\frac{d}{dt}\psi_t(x) = u_t(\psi_t(x_0|x_1)|x_1)$  with initial condition  $\psi_0(x_0|x_1) = x_0$ . This allows the conditional flow matching loss to be reformulated as:

$$\mathcal{L}_{\text{CFM}} = \mathbb{E}_{t, p_1(x_1), p_0(x_0)} [\|v_t(x_t) - \dot{x}_t\|_g^2]. \quad (20)$$

Once trained, samples can be generated by simulating Equation (17) using the learned vector field  $v_t$ .

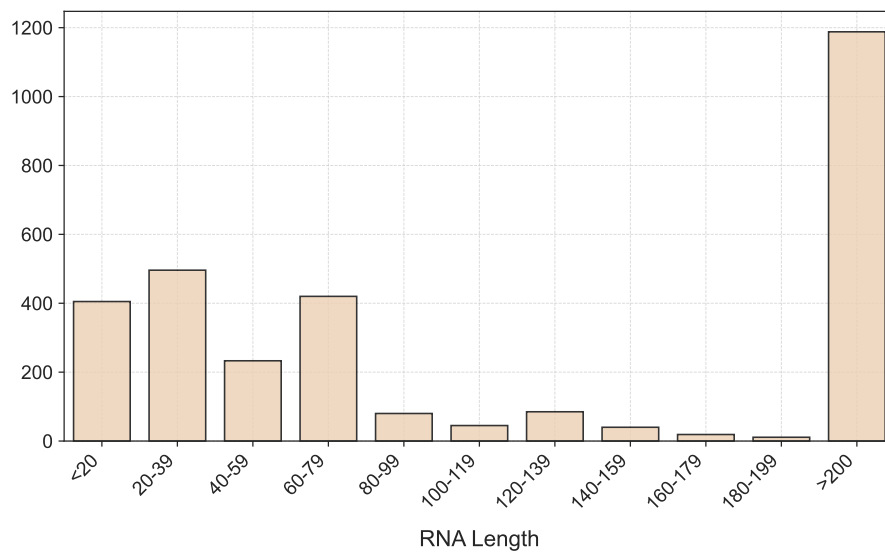
## D. Implementation Details

RiboFlow utilizes several hyperparameters in the experiments, which are crucial for the model’s training and sampling processes. Therefore, we provide some key hyperparameters to facilitate the reproduction of our experiments. The optimal hyperparameters are indicated in bold.

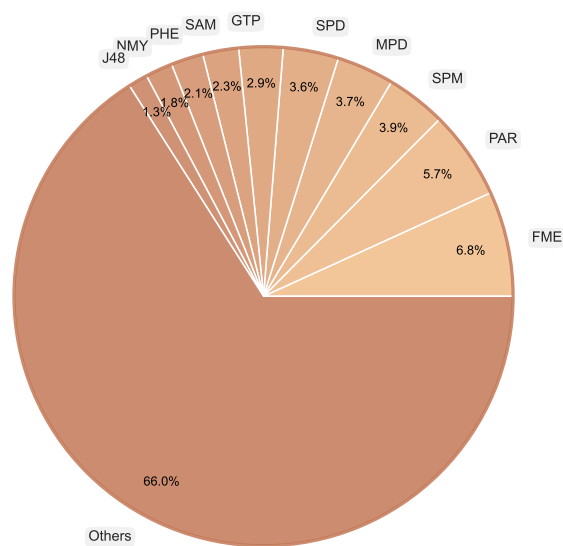


Table S3: Hyperparameters for the RiboFlow.

Category	Hyperparameter	Value
IPA Module	Atom embedding dimension	256
	Hidden dimension	16
	Number of blocks	8
	Query and key points	8
	Number of heads	8
	Key points	12
Transformer	Number of heads	4
	Number of layers	4
Torsion MLP	Input dimension	256
	Hidden dimension	128
Ligand Module	Number of atom type	95
	Number of RBF	16
	Distance range	[0.05, 6.0]
Training Schedule	Translations (training / sampling)	linear / linear
	Rotations (training / sampling)	linear / exponential
	Number of sampling steps	[ <b>50</b> , 100]
	Optimizer	AdamW
	Learning rate	1e-4
	Number of GPUs	4
	Batch size	[4, 8, 16, <b>32</b> ]

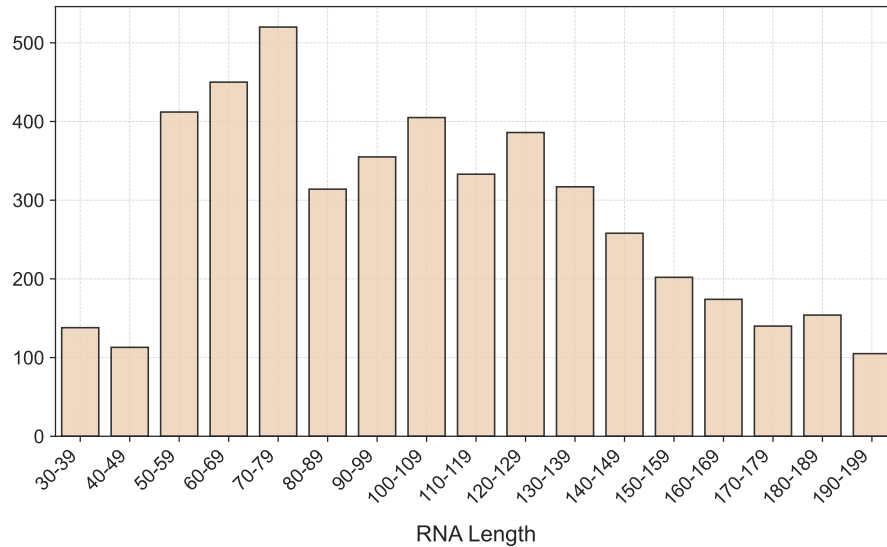


(a) Distribution of RNA Length

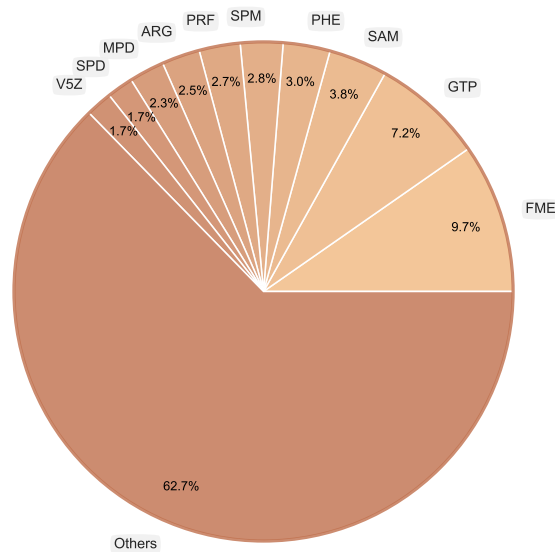


(b) Distribution of Ligand Type

Figure S5: Statistics of the originally collected RiboBind dataset. (a) The number of RNAs within different length ranges, and the vast majority of RNAs exceed the 200-nucleotide limit; (b) The proportion of the top ten categories of ligands.



(a) Distribution of RNA Length



(b) Distribution of Ligand Type

Figure S6: Statistical analysis of the RiboBind dataset, amplified using a *dynamic cropping* strategy after removing sequences shorter than 30 nucleotides, reveals the following: (a) The amplified dataset exhibits a more balanced distribution of RNA lengths compared to the original RiboBind dataset, making it better suited for model training. (b) The top ten ligand categories in the amplified dataset are still predominantly composed of the seven major ligands (FME, GTP, SAM, PHE, SPM, MPD, and SPD) found in the original dataset. This suggests that the ligand bias introduced by the amplification process remains within an acceptable range.

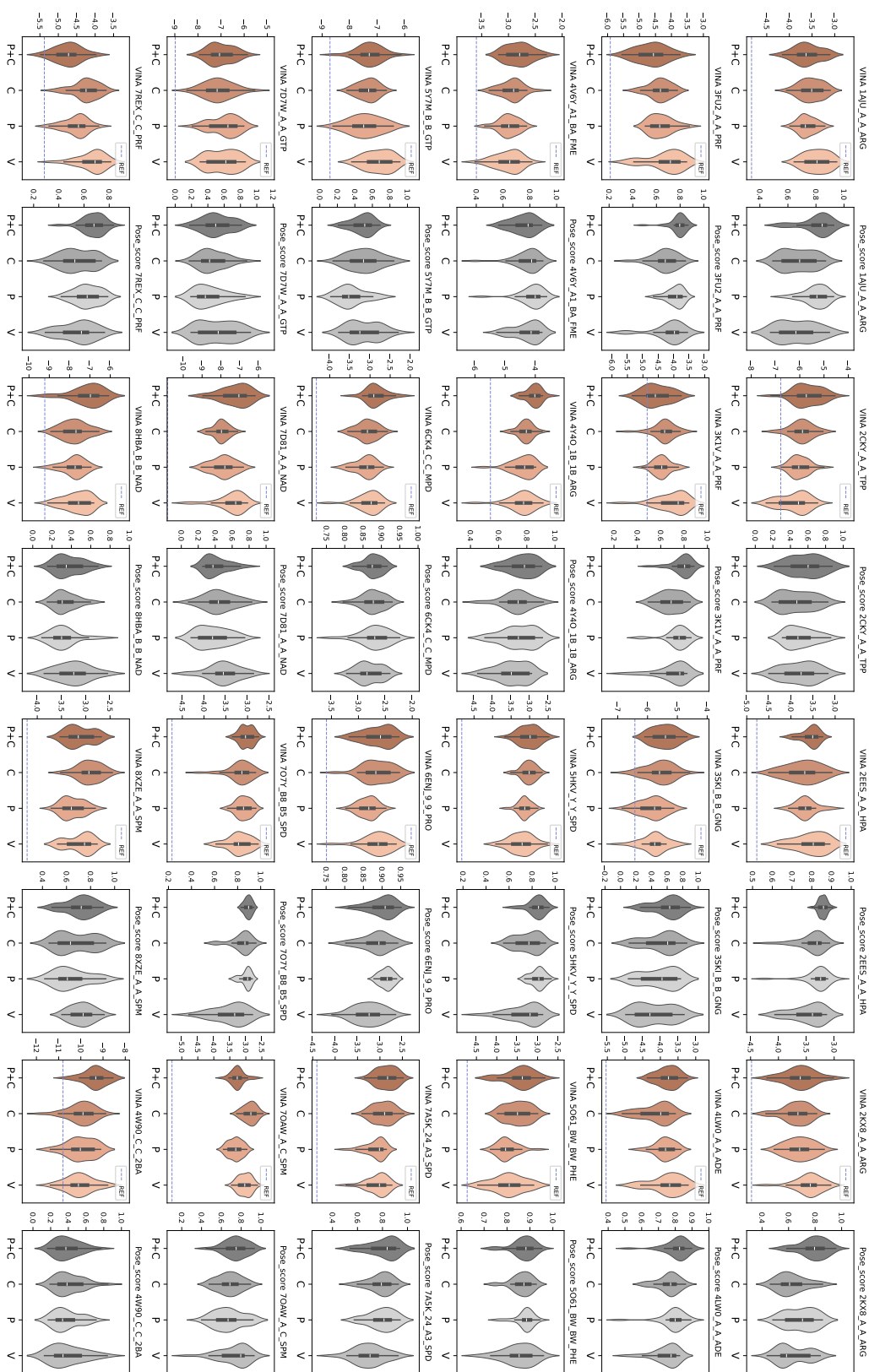


Figure S7: The results of vina and posescore for the 24 RNA-ligand pairs in the standard evaluation set. For vina, we additionally provide the experimental values under real conditions, indicated by a blue dashed line.



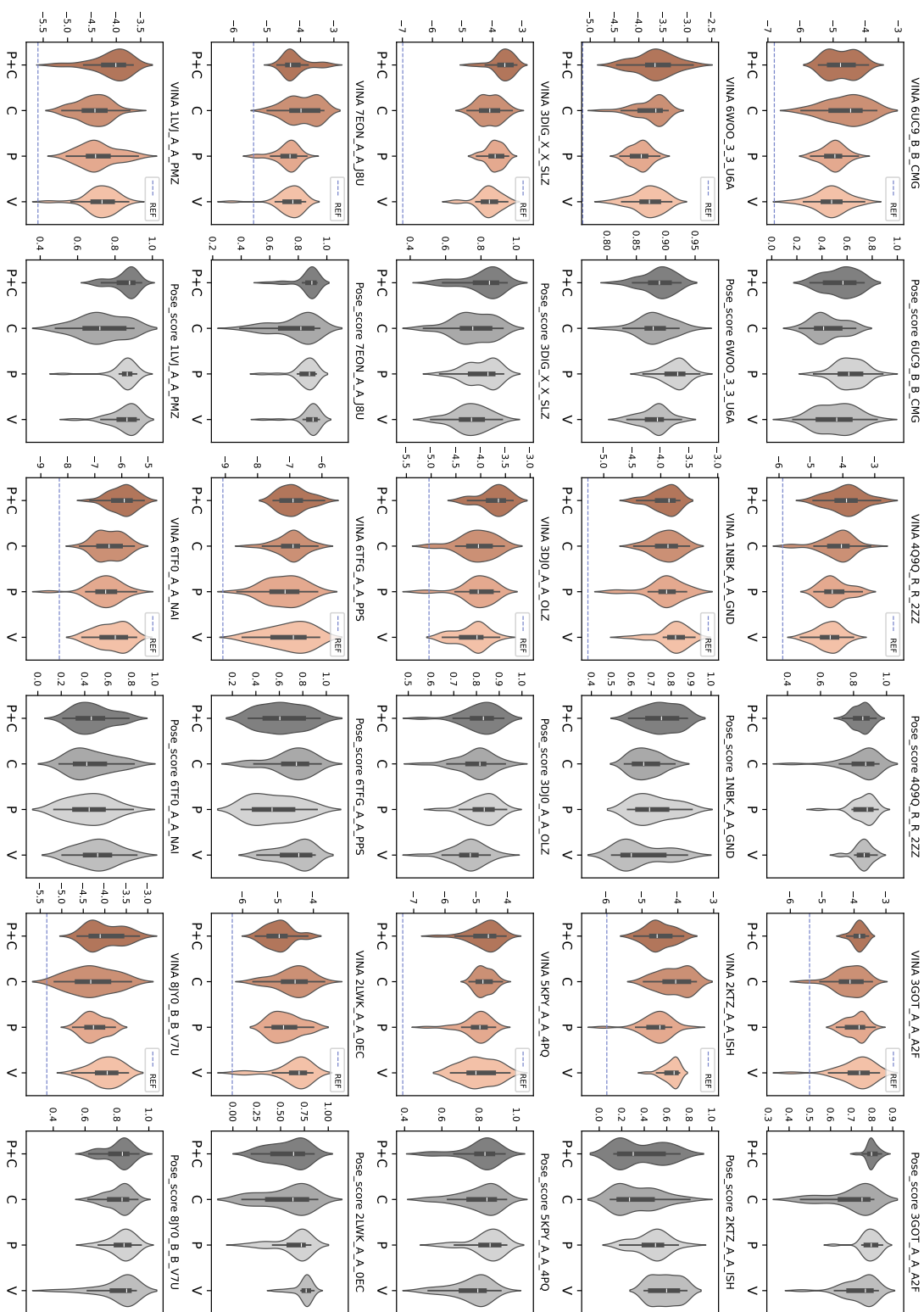


Figure S8: The results of vina and posescore for the 15 RNA-ligand pairs in the few-shot set. For vina, we additionally provide the experimental values under real conditions, indicated by a blue dashed line.